Electronic Supplementary Information (ESI)

Self-assembled three-dimensional hierarchical porous V_2O_5/graphene hybrid aerogels for supercapacitors with high energy density and long cycle life

Yingjie Wu, Guohua Gao* and Guangming Wu*

Shanghai Key Laboratory of Special Artificial Microstructure, Tongji University, Shanghai, 200092, China

E-mail: gao@tongji.edu.cn; wugm@tongji.edu.cn

Experimental Section:

Synthesis of V_2O_5 sol:

Functional V_2O_5 sol was prepared from commercial V_2O_5 powder through heating reflux. In a typical procedure, raw V_2O_5 powder was immersed in benzyl alcohol and isopropanol (molar ration 1:4:40), and then the suspension was heated at 90 °C under a water-cooled condenser for 4 h over which the vanadium oxide (VO_x) oligomers were formed. After filtration, unreacted V_2O_5 was removed for recycling and the pale-yellow V_2O_5 sol was obtained, in which V_2O_5 content was about 40 mg ml^{-1}.

Preparation of V_2O_5/graphene hybrid aerogel:

Graphene oxide (GO) was prepared from natural graphite flakes by a modified Hummers method.[1] GO aqueous dispersion (15 ml) was added into 10 ml as-prepared V_2O_5 sol under vigorous stirring. After about 5 min, VO_x/GO gel was obtained and the gel was then aged for 2 days at 50 °C. The obtained hydrogel was immersed in

acetone to completely replace residual water and solvents. Then, the wet gel was dried using supercritical CO_2 drying or freeze drying to yield the VO_x/GO aerogel. At last, the as-prepared aerogel was annealed in air at 300 °C for 3 h to thermally reduce GO. For comparison, VO_x aerogel (VO_x-Ae) and V_2O_5 aerogel (V_2O_5-Ae) were also obtained under same conditions but absence of GO.

Characterizations:

The morphology of the samples were systematically investigated by field emission scanning electron microscopy (FESEM, S-4800), transmission electron microscopy (TEM, JEOL-2100) and high-resolution transmission electron microscopy (HRTEM, field emission JEOL-2100). X-ray powder diffraction (XRD) pattern was obtained by using a RigakuD/max-C diffractometer with Cu Kα radiation source (λ = 1.5406 Å). Fourier transform infrared spectroscopy (FTIR) was measured using a Bruker-TENSOR27 FTIR spectrometer over the range from 400 to 4000 cm^{-1}. Raman spectra (Jobin-Yvon HR800) was recorded from 100 to 2000 cm^{-1} using a 514 nm argon ion laser. The thermogravimetry analysis (TGA) and differential thermogravimetry analysis (DTG) were carried out on a SDT Q600 over the temperature range from 50 to 650 °C using a heating rate of 10 °C min^{-1} under air atmosphere. Nitrogen adsorption isotherms for calculating the Brunauer-Emmett-Teller (BET) surface area were measured using an Autosorb-1 (Quantachorme) analyzer.

Electrochemical Measurements:

A symmetric two-electrode system was used to measure the electrochemical behavior of as-prepared electrode materials. The electrode was prepared by mixing 80% of the active materials, 10% carbon black and 10% poly (vinylidene fluoride) (PVDF) dispersed in N-methylpyrrolidinone (NMP) to form slurry. The obtained mixture was coated onto graphite papers with an area of 1 cm^2 and then dried at 120 °C for 12 h under vacuum to remove the solvent. The cyclic voltammetry (CV) and galvanostatic charge/discharge measurements were carried out by a CHI 660C electrochemical workstation over the potential range from -1 to 1 V. Electrochemical impedance spectroscopy (EIS) measurements were carried out in a frequency range of 0.01 Hz to 100 kHz with AC amplitude of 5 mV by using CHI 660C electrochemical workstation. The electrolyte used in all of the above measurements was a 1 M Na_2SO_4 aqueous solution. The specific capacitance for a single electrode was calculated from the galvanostatic discharge curves as $C = 2I\Delta t/\Delta V$, where I is the constant discharging current density, Δt is the discharging time and ΔV is the potential window. Energy density and power density were calculated by using the formula $E = 1/8C(\Delta V)^2$ and $P = E/\Delta t$.[2]

Scheme S1. Possible chemical reactions in the formation and hydrolysis of V_2O_5 sol.

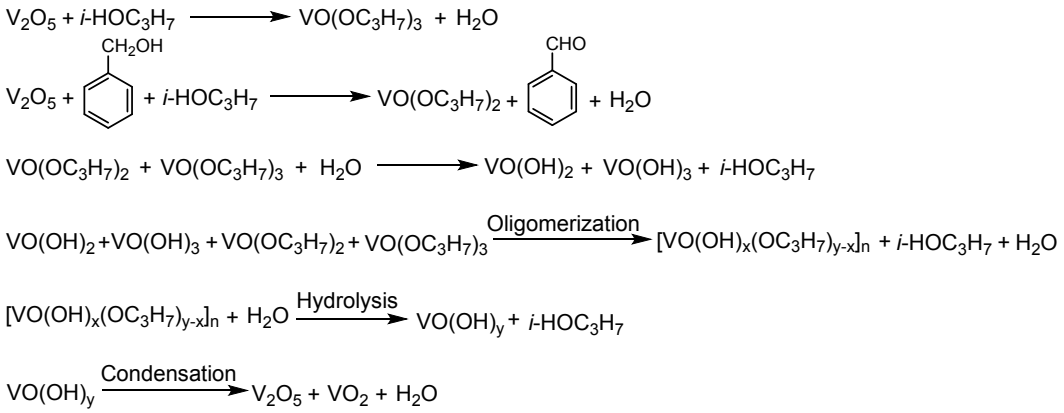

In the process of reaction, benzyl alcohol as a reducing agent and isopropyl alcohol as the solvent, $[VO(OH)_x(OC_3H_7)_{y-x}]_n$ ($3 \geq y \geq 2$, $y \geq x \geq 0$) (for convenience, denoted as VO_x) oligomers are obtained during the complicated chemical reactions.[3] There are lots of V^{4+} in the sol acting as initiator of polymerization and that is why our functional sol is highly active.[4] It is worth noting that, because as-prepared V_2O_5 sol is so sensitive to water that hydrolysis can happen rapidly even in air, it is difficult to make further characterization of our V_2O_5 sol. But the color (light yellow) of sol and final production (V_2O_5) are consist with our hypothesis and demonstrate that V_2O_5 powder is successfully converted into functional V_2O_5 sol, which provides a low-cost alternative for relatively expensive vanadium precursors.[5]

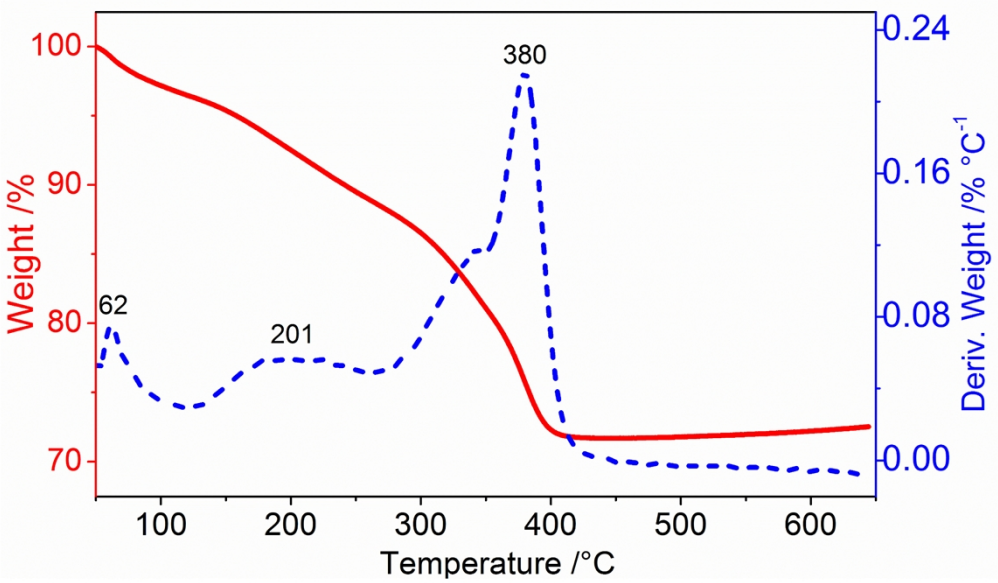

Fig. S1. TGA-DTG curves of V_2O_5/GN hybrid aerogel in air. The weight loss at 62, 201 and 380 °C can be attributed to the evaporation of solvent, decomposition of oxygen-containing functional groups of GO and crystallization of vanadium oxide, respectively.[6, 7] The weight gain after 420 °C is due to the oxidation of low valence V^{4+} to high valence V^{5+} in air, but it does not mean the oxidation reaction only occurs at temperature higher than 420 °C. In fact, 300 °C is enough for the oxidation of V^{4+}, which is corresponding to our experimental results that green VO_x and VO_x/GO aerogel change into yellow V_2O_5 and V_2O_5/GN composite aerogel at 300 °C in air.[8]

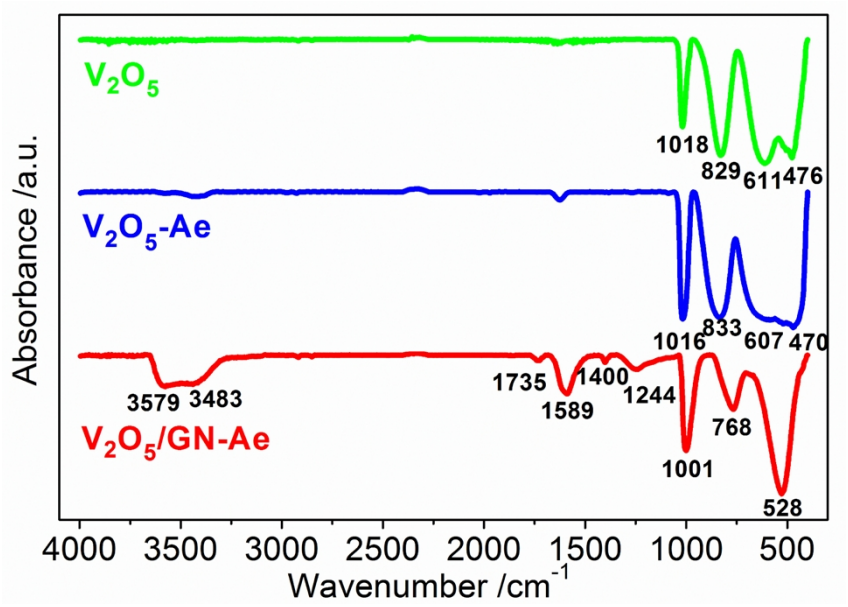

Fig. S2. FTIR spectra of V_2O_5 powder, V_2O_5 aerogel and V_2O_5/GN composite aerogel.

The characteristic peaks of vanadium oxide for V_2O_5 powder appear at 1018, 829, 611 and 476 cm^{-1} are corresponding to the stretching vibration of terminal oxygen bonds (V=O), the vibration of doubly coordinated oxygen (bridge oxygen) bonds and the asymmetric and symmetric stretching vibrations of triply coordinated oxygen (chain oxygen) bonds, respectively.[9] The positon of adsorption peaks for V_2O_5 aerogel are consist with commercial V_2O_5 powder, which clearly demonstrates that the transformation of our functional sol into V_2O_5 is feasible. For V_2O_5/GN aerogel composite, the characteristic adsorption peaks of vanadium oxide are shifted, indicating the strong interaction of V_2O_5 and graphene.[10] The bond at 1589 cm^{-1} is clearly observed, which belongs to the skeletal vibration of graphene sheets.[11]

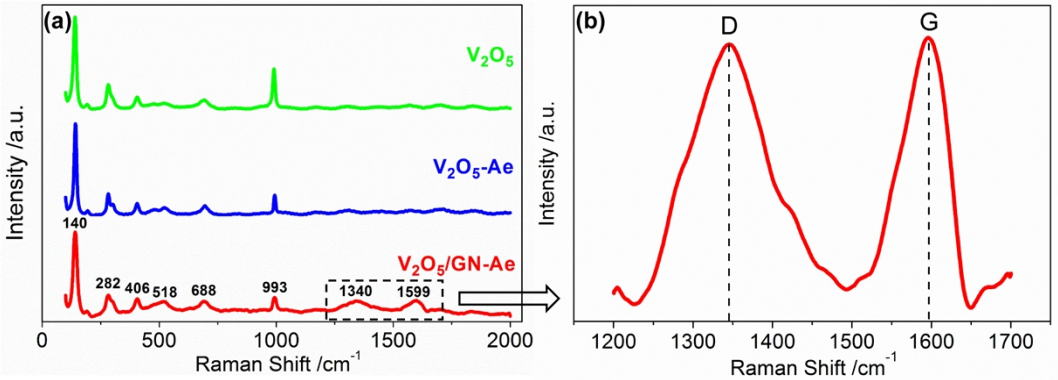

Fig. S3. (a, b) Raman spectra of V_2O_5 powder, as-prepared V_2O_5 aerogel and V_2O_5/GN hybrid aerogel. There are six peaks at 140, 282, 406, 518, 688 and 993 cm^{-1} for both V_2O_5, V_2O_5 aerogel and V_2O_5/GN hybrid aerogel corresponding to the skeleton bending vibration of the V-O-V bonds, bending vibrations of V=O bonds, bending vibrations of bridge oxygen bonds, stretching vibrations of triply coordinated oxygen bonds, stretching vibrations of doubly coordinated oxygen and in-phase stretching vibrational of V=O bonds, respectively.[10] These same characteristic peaks of V_2O_5 indicate the presence of V_2O_5 in the three materials. In addition, for V_2O_5/GN composite aerogel, the characteristic D and G bands of graphene also appear at 1340 and 1599 cm^{-1}, respectively.[12] Thus, the reduction of graphene oxide and incorporation with V_2O_5 are confirmed.

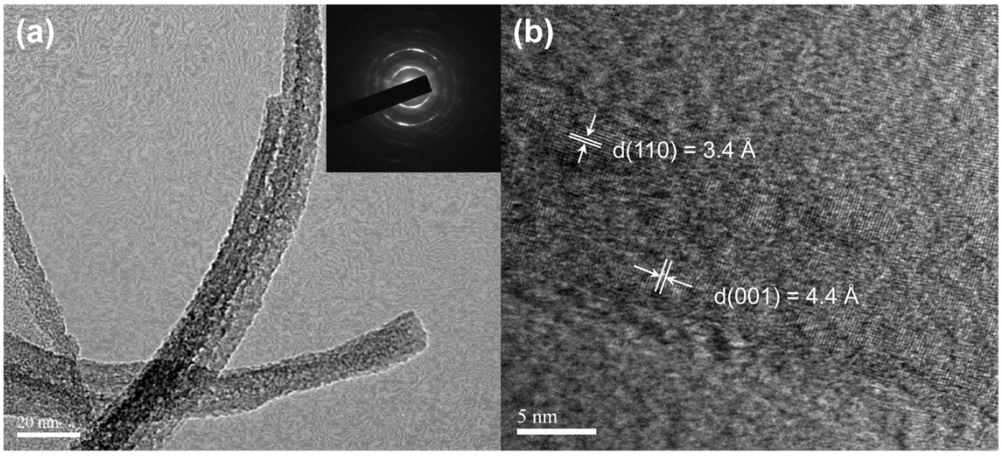

Fig. S4. (a) TEM image and SAED patterns (inset) of VO_x nanofibers. These fibers with length of several micrometers and dozens of nanometers in diameter are noncrystalline. (b) High-resolution TEM (HRTEM) image of V_2O_5 nanofibers. The distinct lattice fringes further confirm partly crystallization of V_2O_5 during thermal treatment.

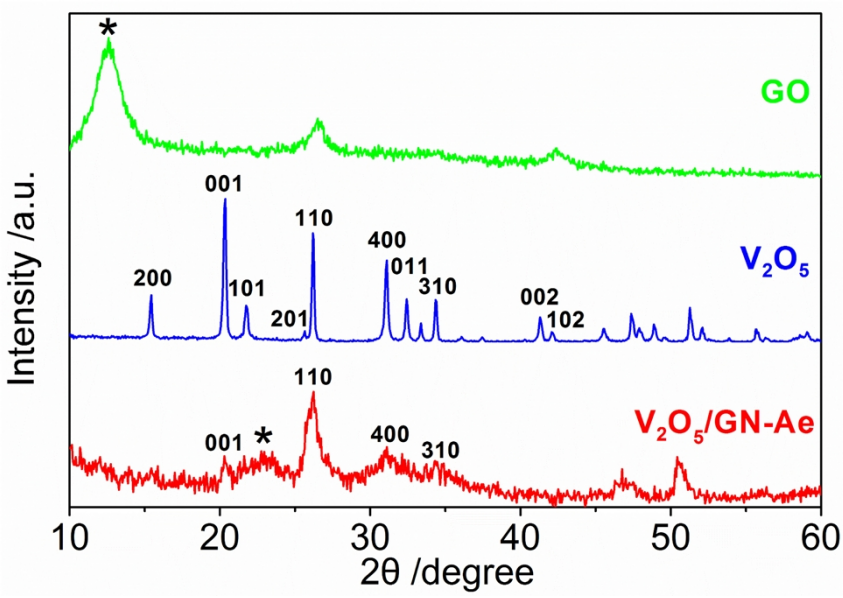

Fig. S5. XRD patterns of graphene oxide (GO), raw V_2O_5 powder and V_2O_5/GN hybrid aerogel. The commercial V_2O_5 powder has an orthorhombic structure (JCPDS no. 41-1426). The XRD patterns of V_2O_5/GN composite aerogel exhibit a (002) reflection peak of graphene at 23°, which suggests that graphene sheets in the composite aerogel are few layers thick.[13] Besides, the presence of (001), (110), (400) and (310) reflection peaks of V_2O_5 indicates that the obtained hybrid aerogel is partly crystalline after thermal treatment, which is consist with the results of thermogravimetric analysis.

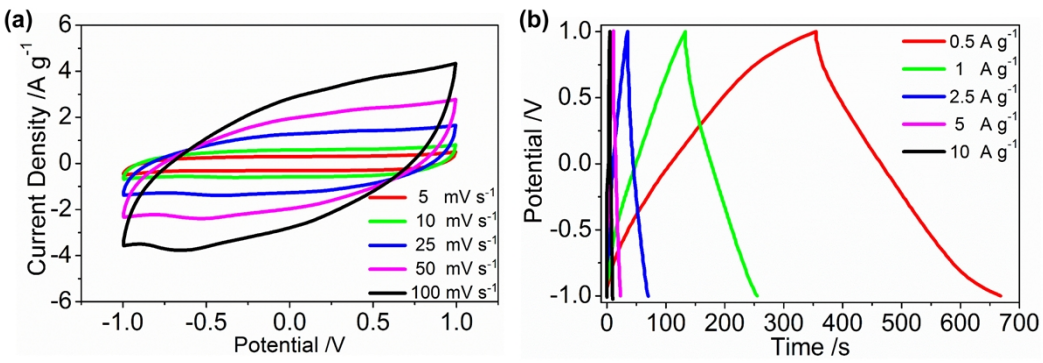

Fig. S6. (a) CV curves of V_2O_5 powder tested at different scan rates and (b) Galvanostatic charge/discharge of V_2O_5 powder evaluated at different current densities.

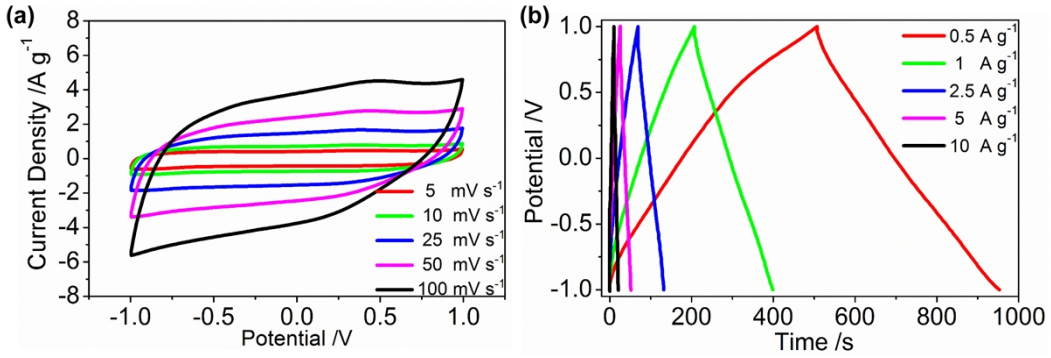

Fig. S7. (a) CV curves of V_2O_5 aerogel tested at different scan rates and (b) Galvanostatic charge/discharge of V_2O_5 aerogel evaluated at different current densities.

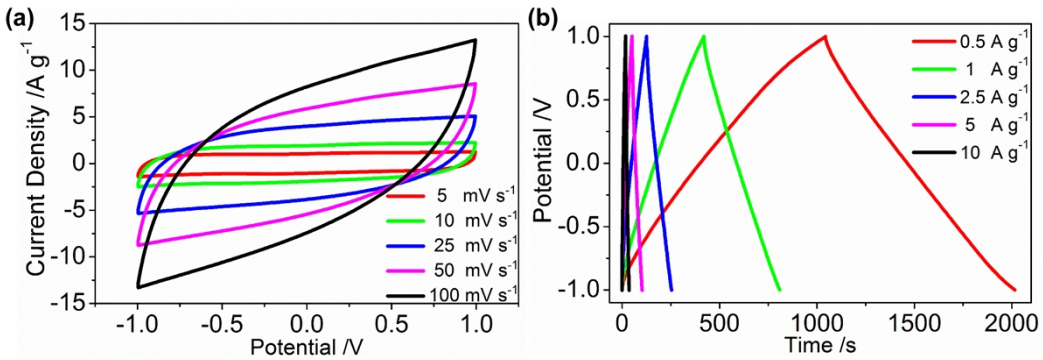

Fig. S8. (a) CV curves of V_2O_5/GN composite aerogel tested at different scan rates and (b) Galvanostatic charge/discharge of V_2O_5/GN aerogel evaluated at different current densities.

References:

1 W. S. Jr. Hummers and R. E. Offeman, *J. Am. Chem. Soc.*, 1958, **80**, 1339.

2 L. L. Zhang, X. Zhao, M. D. Stoller, Y. W. Zhu, H. X. Ji, S. Murali, Y. P. Wu, S. Perales, B. Clevenger and R. S. Ruoff, *Nano Lett.*, 2012, **12**, 1806.

3 M. K. Atal, V. Dhayal, M. Nagar, R. Bohra, K. S. Rathore and N. S. Saxena, *J. Sol-Gel Sci. Technol.*, 2010, **53**, 67.

4 J. Livage, *Chem. Mater.*, 1991, **3**, 578.

5 J. Livage, *Solid State Ionics*, 1996, **86**, 935.

6 S. Stankovich, D. A. Dikin, R. D. Piner, K. A. Kohlhaas, A. Kleinhammes, Y. Y. Jia, Y. Wu, S. T. Nguyen and R. S. Ruoff, *Carbon*, 2007, **45**, 1558.

7 X. W. Zhou, G. M. Wu, G. H. Gao, J. C. Wang, H. Y. Yang, J. D. Wu, J. Shen, B. Zhou and Z. H. Zhang, *J. Phys. Chem. C*, 2012, **116**, 21685.

8 Z.-L. Wang, D. Xu, Y. Huang, Z. Wu, L.-M. Wang and X.-B. Zhang, *Chem. Commun.*, 2012, **48**, 976.

9 X. W. Zhou, G. M. Wu, J. D. Wu, H. Y. Yang, J. C. Wang, G. H. Gao, R. Cai and Q. Y. Yan, *J. Mater. Chem. A*, 2013, **1**, 15459.

10 H. W. Wang, H. Yi, X. Chen and X. F. Wang, *J. Mater. Chem. A*, 2014, **2**, 1165.

11 J. L. Wang, Z. X. Shi, J. C. Fan, Y. Ge, J. Yin and G. X. Hu, *J. Mater. Chem.*, 2012, **22**, 22459.

12 Y. W. Zhu, S. Murali, W. W. Cai, X. S. Li, J. W. Suk, J. R. Potts and R. S. Ruoff, *Adv. Mater.*, 2010, **22**, 3906.

13 H. Hu, Z. B. Zhao, W. B. Wan, Y. Gogotsi and J. S. Qiu, *Adv. Mater.*, 2013, **25**, 2219.